Electrochemical preparation of iron cuboid nanoparticles and their catalytic properties for nitrite reduction

Yan-Xin Chen, Sheng-Pei Chen, Qing-Song Chen, Zhi-You Zhou, Shi-Gang Sun [*],[1]

State Key Lab of Physical Chemistry of Solid Surfaces, Department of Chemistry, College of Chemistry and Chemical Engineering, Xiamen University, Xiamen 361005, China

ARTICLE INFO

ABSTRACT

Iron cuboid nanoparticles supported on glassy carbon (denoted nm-Fe/GC) were prepared by electrochemical deposition under cyclic voltammetric (CV) conditions. The structure and composition of the Fe nanomaterials were characterized by scanning electron microscopy (SEM), selected area electron diffraction (SAED), X-ray diffraction (XRD) and energy dispersive X-ray analysis (EDX). The results demonstrated that the Fe cuboid nanoparticles are dispersed discretely on GC substrate with an average size ca. 171 nm, and confirmed that the electrochemical synesized nanocubes are single crystals of pure Fe. The catalytic properties of the Fe cuboid nanoparticles towards nitrite electroreduction were investigated, and enhanced electrocatalytic activity of the Fe nanocubes has been determined. In comparison with the data obtained on a bulk-Fe electrode, the onset potential of nitrite reduction on nm-Fe/GC is positively sifted by 100 mV, and the steady reduction current density is enhanced about 2.4–3.2 times.

1. Introduction

As a result of small size effect, surface effect and other peculiar physicochemical effects, nanomaterials exhibit novel properties and have attracted considerable attentions in diverse fields such as optics, electronics, catalysis, and magnetic data storage [1–3], etc. The nanostructured materials have also played important roles in corrosion, fuel cells, and photochemistry due to their ease of preparation, high catalytic activity and low cost [4–7].

Fe is an important member of the iron-triad elements and belongs to the body centered crystal (bcc) system. The Fe materials are important catalysts in ammonia synthesis [8–11] and denitrification [12–14]. Somorjai et al. have demonstrated that the surface structure of Fe catalysts have a significant impact on their activity [8,10]. For the iron-catalyzed ammonia synthesis reaction, the $(1\,1\,1)$ plane of a Fe single crystal was found to be the most active, and the activity ratio was obtained to be 418:25:1 for the Fe$(1\,1\,1)$, Fe$(1\,0\,0)$ and Fe$(1\,1\,0)$ [8]. Recently, extensive studies were carried out to synthesize Fe nanoparticles for different applications [15–17]. It is well known that the surface structure of nanoparticles can be tuned by shape control synthesis [18]. Song et al. [19] illustrated that Pt nanoparticles of cubes, cuboctahedra and octahedra can be obtained by chemical synthesis through well controlling the conditions. For these shapes of Pt nanoparticles, the corresponding surface structures are $\{1\,0\,0\}$, $\{1\,0\,0\}+\{1\,1\,1\}$ and $\{1\,1\,1\}$, respectively. Recently, Tian et al. [20] have developed an electrochemical method to control the shape of Pt nanoparticles. In their work, tetrahexahedral Pt nanoparticles bounded with $\{7\,3\,0\}$, $\{5\,2\,0\}$ and vicinity high-index facets were obtained, and exhibited high catalytic activity and stability. In concerning the shape control synthesis of Fe nanoparticles, the hollow Fe nanocubes and nanoframes [21,22], α-Fe$_2$O$_3$ naocubes [23] and α-Fe$_2$O$_3$ rhombohedral nanoparticles [24] were obtained by chemical synthesis routes.

In today's society, the intensive use of fertilizers in agriculture and nitrates in some industrial sectors causes a severe nitrate pollution of water sources and industrial sites. Because nitrate becomes toxic once it is converted to nitrite by the reducing action of bacteria in the human body, the development of denitrification technology is therefore an important issue in environment and human being health. It exists a few technologies such as biological denitrification, ion-exchange, reverse osmosis, as well as chemical and catalytic reductions. In comparison, the electrochemical denitrification has received increasing attentions because it has superior advantages regarding environmental compatibility, versatility, energy efficiency, safety, selectivity, amenability and cost effectiveness [25]. The electroreduction of nitrate and nitrite has been conducted on different electrodes, such as Cu modified Au [26], brass (Cu$_{60}$Zn$_{40}$) screen [27], Rh-modified pyrolytic graphite [28], Sn-modified Pt [29], Pd/Sn/Au electrodes [30], copper thallium [31], Cu$(1\,0\,0)$ [32], Pd-based bimetallic supported catalysts [33], polypyrrole nanowires modified graphite [34], and Fe catalysts [35,36]. The

* Corresponding author. Fax: +86 592 2183047.
E-mail address: sgsun@xmu.edu.cn (S.-G. Sun).
[1] ISE member.

electroreduction of nitrate and nitrite has contributed also in the nitrogen cycle that has attracted much attention in recent years because of its ecological importance concerning the widespread agricultural use of potentially polluting nitrate and nitrite.

In the current paper, Fe cuboid nanoparticles supported on glassy carbon were prepared by an electrochemical method. The study has illustrated that the Fe nanocubes exhibit enhanced electrocatalytic activity towards nitrite reduction, which is ascribed not only to the nanosize effect but also the surface structure effect of the nanocubes that are bounded by bcc {1 0 0} facets of open structure.

2. Experimental

2.1. Preparation of Fe cuboid nanoparticles

Glassy carbon substrate (GC, 6.0 mm in diameter with a geometric area of 0.28 cm^2) was sealed into a Teflon holder and polished mechanically using successively sand paper (6#) and alumina powder of size 5, 1, 0.3, and 0.05 μm before metal deposition. A polycrystalline Fe rod (99.995%, Alfa) of 5 mm in diameter sealed into a Teflon holder with a geometric area of 0.2 cm^2 was polished mechanically using the same procedure and served as a reference surface of bulk-Fe electrode in the study. The Fe cuboid nanoparticles were deposited electrochemically onto GC substrate under cyclic voltammetric (CV) conditions in 0.02 mol L^{-1} FeSO$_4$ solution. Ten cycles of potential cycles was applied in the deposition with potential cycling between −0.9 and −1.25 at a scan rate 50 mV s^{-1}. The electrode after Fe deposition was denoted thereafter as nm-Fe/GC. Before each electrochemical measurement, both the bulk-Fe and the nm-Fe/GC electrode were subjected to a cathodic polarization at −1.25 V for 15 min in 0.2 mol L^{-1} NaOH solution, in order to reduce possible oxide on the surface and activate the electrode for further studies. An EG&G potentiostat/galvanostat (model 263A) was used in electrochemical studies. A commercial saturated calomel electrode (SCE) and a platinized platinum foil were served as reference electrode and counter electrode, respectively. The potentials reported in this paper are referred to the SCE scale. The solutions were prepared with Millipore water (18 MΩ cm) provided by a Milli-Q Labo apparatus (Nihon Millipore Ltd.). The chemicals are Alfa Aesar reagents of FeSO$_4$, NaNO$_2$ and NaOH. The solutions were deaerated by bubbling high-purity N$_2$ before measurements. All experiments were carried out at room temperature.

2.2. SEM, XRD and HRTEM characterizations

The freshly prepared Fe nanoparticles deposited electrochemically on GC substrate (nm-Fe/GC) was taken out from solution at reduction potential after their preparation, and then protected in absolute alcohol to carry them to the characterizations. The morphology of the nm-Fe/GC was studied by scanning electron microscopy (SEM, LEO l530) that operated at 20 kV. Powder samples of Fe nanoparticles, which were taken from the nm-Fe/GC surface, were examined by powder X-ray diffraction (XRD) on an Analytical X'pert PRO diffractometer. Analysis of transmission electron microscopy (TEM) and high-resolution transmission electron microscopy (HRTEM) was conducted on instruments of JEM-100CX- II and FEI Tecnai-F30, respectively.

2.3. Investigation of nitrite reduction on nm-Fe/GC and on bulk-Fe electrodes

The investigation of NO$_2^-$ reduction was carried out in 0.2 mol L^{-1} NaOH containing 0.01 mol L^{-1} NaNO$_2$ (Alfa Aesar) solutions. The potential range in cyclic voltammetric studies was from −1.0 to −1.35 V. In order to demonstrate the differences in steady catalytic activity between nm-Fe/GC and bulk-Fe electrodes, j–t curves were recorded on the two electrodes, respectively, at −1.2, −1.25 and −1.3 V within a time window of 300 s.

3. Results and discussion

3.1. Preparation and electrochemical characterization of nm-Fe/GC electrode

Cyclic voltammograms recorded during Fe electrodeposition on GC in 0.02 mol L^{-1} FeSO$_4$ solution is displayed in Fig. 1. In the first cycle, the reduction current (negative current) remains small till −1.23 V in the negative-going potential scan (NGPS), it is then increased quickly. The reduction current is continuously increasing in the reverse potential scan until −1.23 V then is decreased progressively. A fast increase in the cathodic current is observed in the second cycle, and the cathodic current is even larger than that of the first cycle. A broad current peak around −1.05 V is seen in the NGPS of the third cycle, the value of the reduction current is still compatible with those in the first and the second cycles. Starting from the fourth cycle the broad current peak is shifted to positive potential direction, and the cathodic current is decreased gradually. These results may imply that the nucleation of Fe on GC surface is difficult, and that the growth of Fe particles is much fast once the Fe nuclei were formed, similar to the case of electrodeposition of Co nanoparticles [37].

In general, for heterogeneous nucleation, to obtain individual particles or clusters, the surface energy of the substrate (working electrode) should be much small than that of the deposits, which leads to island formation through a Volmer–Weber growth mode [38]. It is known that the surface energy of the substrate (Glass Carbon) is much smaller than that of the deposits (Fe). It is evident that in the second NGPS, Fe could nucleate either on Glass Carbon or deposit on Fe nucleates that are formed in the first potential cycle. Along with increasing the number of potential cycling, Fe nucleates produced on GC surface are increased. As a consequence, in successive potential cycles, most nucleation will take place on Fe nucleates. The fact that the peak current at −1.05 V is continuously decreasing along with the increase of the potential cycling number may be interpreted as follows. On the one hand, as stated above, along with increase of the number of potential cycles more and more Fe nucleates are formed on GC surfaces, therefore the process become progressively the growth of Fe particles. On the other hand, the possibility of Fe deposition on Fe particles is increasing, which
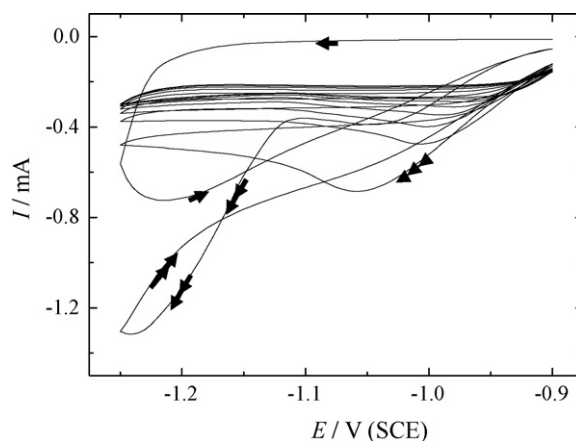

Fig. 1. Cyclic voltammograms of electrodeposition of Fe on GC electrode, 0.02 mol L^{-1} FeSO$_4$ solutions, scan rate 50 mV s^{-1}.
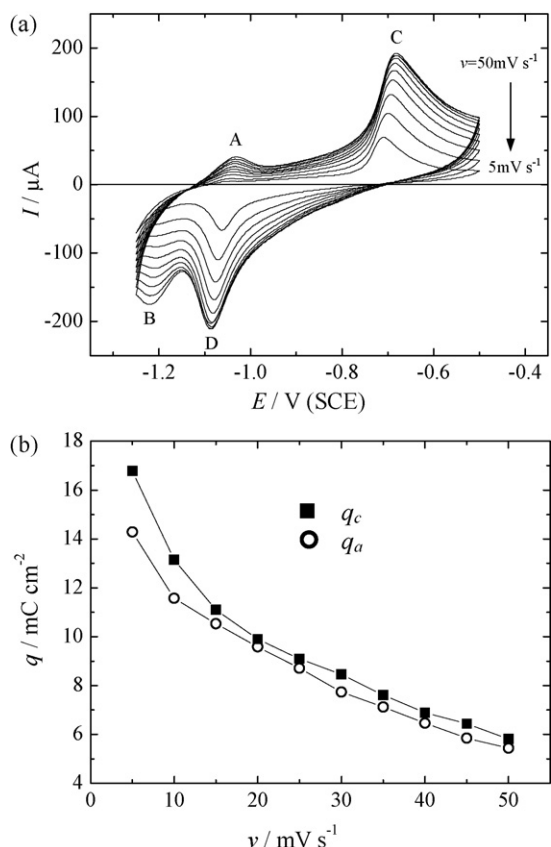
Fig. 2. (a) Cyclic voltammograms of bulk-Fe electrode recorded at different scan rates varying from 50 to 5 mV s^{-1}, 0.2 mol L^{-1} NaOH solution; (b) variations of electric charge densities with scan rate.

Fig. 3. Cyclic voltammograms of bulk-Fe electrode, 0.2 mol L^{-1} NaOH solution, scan rate 25 mV s^{-1}, with potential scan range of −1.25 to −0.5 V(. . . . . .) and −1.1 to −0.5 V (−).

leads to reach the diffusion control since the Fe ions near electrode surface could be used up quickly.

In concerning the determination of the electroactive surface area of the nm-Fe/GC electrode, the data of the bulk-Fe electrode was served as a reference. It is known that the Fe electrode in alkaline solutions under electrochemical conditions will undergo oxidation and passivation processes, i.e. multilayer of Fe oxide will be formed on the surface. This differs significantly from the adsorption/desorption process on Pt or other noble metal electrodes, in which the density of electric charge corresponding to the adsorption/desorption is limited and well defined. For example, in the case of hydrogen adsorption on a polycrystalline Pt electrode, a value of 210 μC cm^{-2} is generally accepted. However, the density of electric charge measured with a Fe electrode will depend on the degree of passivation of Fe surface or the number of Fe oxide layers formed.

In order to illustrate this effect, we have investigated the influence of potential scan rate (v) on the density of electric charge using the bulk-Fe electrode in 0.2 M NaOH solution within a fixed potential scan range between −1.25 and −0.5 V. Two pairs of current peak (A vs. B, and C vs. D) are observed in all cyclic voltammograms shown in Fig. 2a. It can be observed that the formation of a surface oxide film begins at around −1.10 V in the anodic potential scan, which is depicted by the anodic current, i.e. the current above the zero line. Two oxidation current peaks are appeared near −1.03 (A) and −0.69 (C). In the cathodic potential scan two reduction current peaks are observed close to −1.09 (D) and −1.21 V (B). The anodic process may correspond to electrooxidation of Fe into the Fe(II) and Fe(III) species [39], which may be FeOOH and some hematite and maghemite, as have been determined both by UV–vis potential-modulated reflectance spectroscopy [41] and by UV–vis
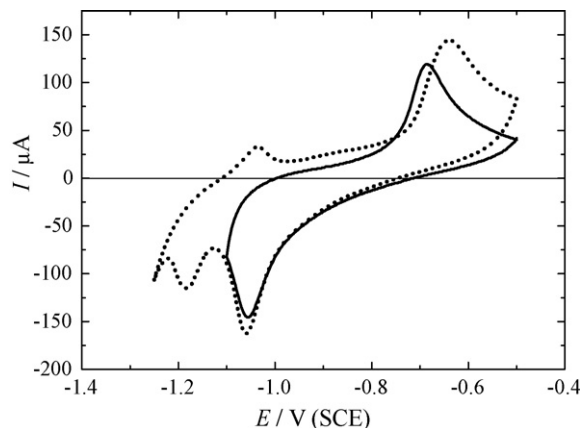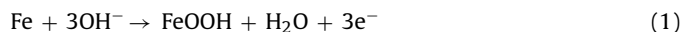
differential reflectance spectroscopy [42]. So the oxidation of Fe surface in alkaline solutions may be described as [43]:

$$Fe + 3OH^- \rightarrow FeOOH + H_2O + 3e^- \tag{1}$$

It can be seen clearly that the current of the two pairs of current peak is decreased progressively when the potential scan rate is increasing. The anodic electric charge density (q_a) as well as the cathodic one (q_c) were measured by integration of CV curves recorded at each v, and plotted in Fig. 2b. It can observe that along with increasing v from 5 to 50 mV s^{-1}, both q_a and q_c are decreased gradually. Taken a value of 807 μC cm^{-2} for a monolayer of Fe(III) oxide formed on a Fe(1 1 0) surface (the most dense atomic arrangement for the three basal planes of bcc system), about 17.6 layers (14.2 mC cm^{-2}) of Fe(III) oxide was estimated to be formed in the anodic scan at v = 5 mV s^{-1}, while only about 6.7 layers (5.4 mC cm^{-2}) of Fe(III) oxide was produced at v = 50 mV s^{-1}. It is worthwhile notifying that q_c is always larger than q_a, especially when v is bellow 15 mV s^{-1}, which indicates that the hydrogen evolution reaction has been occurred in at low potential region within this range of potential cycle.

Fig. 3 presents a typical cyclic voltammogram recorded between −1.25 and −0.50 V for a bulk-Fe electrode in 0.2 mol L^{-1} NaOH aqueous solutions at 25 mV s^{-1}. The CV features are similar to those reported in literature [39,40]. In order to minimize hydrogen evolution reaction and thus to calibrate the electroactive surface area of the nm-Fe/GC using the electric charge density measured on bulk-Fe electrode, a cyclic voltammogram recoded between −1.1 and −0.5 V is also displayed in Fig. 3. Only the pair of current peak appearing at −0.69 V (anodic scan) and −1.06 V (cathodic scan) is observed in the voltammogram. The Q_a is measured at 995 μC, and Q_c is 1061 μC. The average electric charge density $q_{average}$ is thus obtained to be 5.14 mC cm^{-2} ((995 + 1061)/2/0.20) under this condition on the bulk-Fe electrode.

In Fig. 4, a cyclic voltammogram recorded between −1.25 and −0.50 V for the nm-Fe/GC electrode in 0.2 mol L^{-1} NaOH aqueous solutions at 25 mV s^{-1} is compared with the voltammogram recorded on GC substrate electrode under the same conditions. The current recorded on GC electrode is very small in comparison with that on the nm-Fe/GC, implying that the GC surface is inert. The CV of the nm-Fe/GC presents similar features to those observed in the CV of the bulk-Fe electrode, indicating that the same oxidation/passivation processes were occurred on nm-Fe/GC surface. However, it seems that the hydrogen evolution is less significant on nm-Fe/GC, since there is no significant negative current observed at −1.25 V as seen in the CV of bulk-Fe electrode shown in Fig. 3. In
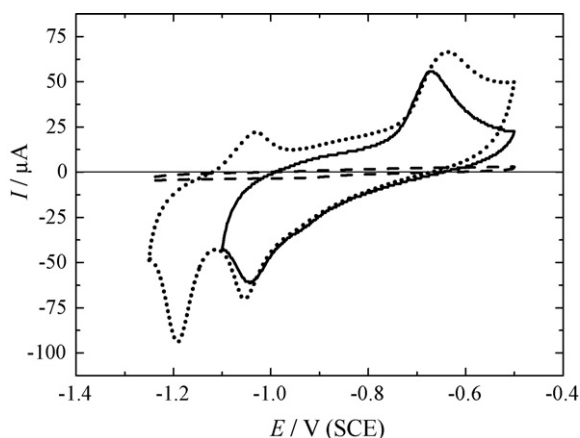
Fig. 4. Cyclic voltammograms of nm-Fe electrode and GC electrode, 0.2 mol L^{-1} NaOH solution, scan rate 25 mV s^{-1}, with potential scan range of −1.25 to −0.5 V(. . . . . .) and −1.1 to −0.5 V (—). The potential scan range of GC electrode was between −1.25 and −0.5 V (- - -).

the same way, the cyclic voltammogram between −1.1 and −0.5 V was recorded on nm-Fe/GC and served to measure electric charge density for estimation of electroactive surface area of nm-Fe/GC. Q_a and Q_c measured from that voltammogram are, respectively, 493 and 494.9 μC, yielding an average value 494 μC. The electroactive surface area of the nm-Fe/GC is therefore evaluated as 0.096 cm^2 (=0.494 mC/5.14 mC cm^{-2}). It is worthwhile to note that the value 0.096 cm^2 is smaller than the geometric area of the GC substrate (0.28 cm^2), which may be interpreted by that the Fe nanoparticles were deposited dispersedly on GC surface and the quantity of Fe

nanoparticles is far from the formation of a monolayer as can be seen from SEM image of the nm-Fe/GC electrode (see Fig. 5 in next paragraph)

3.2. Characterization of nm-Fe/GC by SEM, SAED, EDX and XRD

A SEM image of freshly prepared nm-Fe/GC is presented in Fig. 5a. It illustrates that the Fe nanoparticles are of cubic shape and distributed discretely on the GC surface. The insert to this figure is a magnified image of the Fe nanoparticles, which demonstrates clearly that the Fe nanoparticles are well-defined cubes. From the pattern of selected-area electron diffraction (SAED) shown in Fig. 5b, it confirms that the Fe nanocubes are single crystals matching with the body-centered cubic crystal system. Fig. 5c depicts the histogram of size distribution of the Fe nanoparticles on GC substrate as illustrated in Fig. 5a, indicating that the average size of the Fe nanocubes is 171 nm ± 22 nm with a relative standard deviation (R.S.D.) of 13%.

The chemical composition of the as-prepared Fe nanoparticles is determined by EDX analysis, for which a spectrum is shown in Fig. 6a. The elemental signatures obtained are identical within experimental accuracy, and essentially Fe is determined, as expected. The Cu and C signals are attributed to the HRTEM grid [24]. Fig. 6b presents a typical X-ray diffraction spectrum of the Fe nanocubes. Diffraction peaks are appeared at 44.67°, 65.02°, 82.33°, 98.95° and 116.39°, corresponding, respectively, to diffraction lines of (1 1 0), (2 0 0), (2 1 1), (2 2 0) and (3 1 0) planes. All the observed diffraction peaks can be assigned to those of pure Fe in good agreement with standard data, i.e. Joint Committee for Powder Diffraction Standards (JCPDS) 00-006-0696.
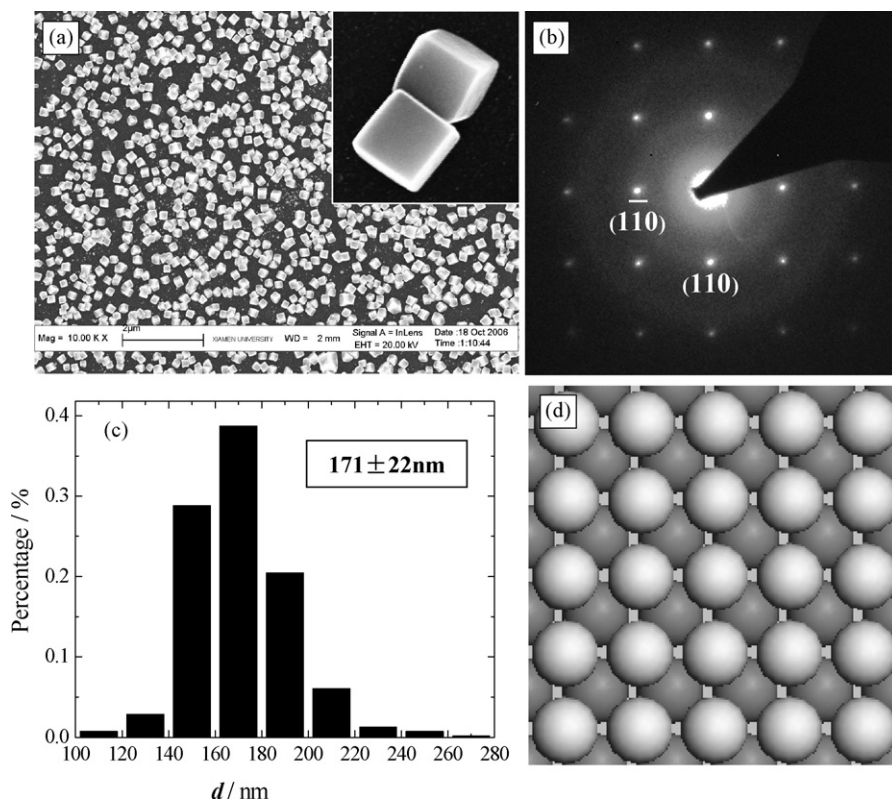

Fig. 5. (a) A typical SEM image of nm-Fe/GC electrode, the insert to this figure illustrates two Fe nanocubes with high magnification; (b) SAED pattern of a single Fe cube; (c) Histogram of size distributions of Fe nanocubes on GC substrate; (d) Model of bcc {1 0 0} plane that shows the open surface structure of Fe nanocubes.
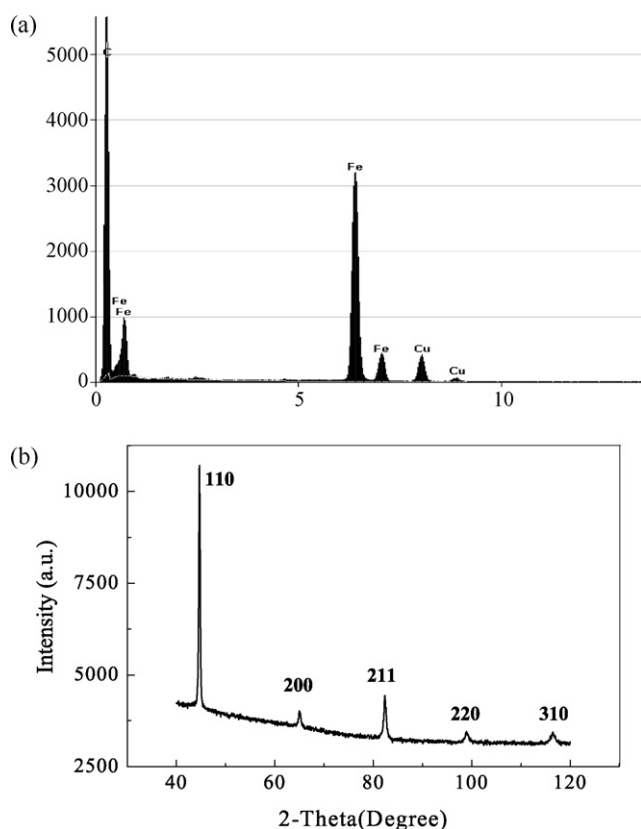
Fig. 6. EDX (a) and XRD (b) spectra of Fe nanocubes.

The above results demonstrated clearly that no Fe oxide species were determined when the sample was protected in absolute alcohol after its preparation taking out from solution at reduction potential, and that the Fe nanoparticles prepared by electrodeposition under present cyclic voltammetric conditions are Fe single crystals of cube shape. It is known that the surfaces of the Fe nanocubes are {1 0 0} facets. A model of bcc {1 0 0} plane of Fe single crystal is represented by Fig. 5d. It is interesting to see that the bcc {1 0 0} exhibits a quite open structure. Such open surface structure will yield in general high catalytic activity [8,20,44]. Therefore, the Fe cuboid nanoparticles are expected to exhibit a good catalytic property that is investigated in following section.

3.3. Catalytic activity of nm-Fe/GC for NO_2^- reduction in alkaline medium

The reduction current has been normalized using the electroactive surface area, so that the current density (j) can be directly used to compare the catalytic activity of the nm-Fe/GC and the bulk-Fe electrodes. The j–E curves of NO_2^- reduction on nm-Fe/GC and bulk-Fe electrodes recorded in solutions of $0.2\,mol\,L^{-1}$ NaOH containing $0.01\,mol\,L^{-1}$ $NaNO_2$ and with a slow potential scan rate of $1\,mV\,s^{-1}$ are compared in Fig. 7. It can be observed clearly that the nitrite reduction starts at about $-1.08\,V$ on nm-Fe/GC electrode, while this reduction is postponed to $-1.18\,V$ on bulk-Fe electrode. The nitrite reduction on nm-Fe/GC yields two distinct current peaks at around -1.18 and $-1.28\,V$, with peak current densities of 7.5 and 8.8 $mA\,cm^{-2}$, respectively. In comparison, the reduction on bulk-Fe yields a current peak near $-1.25\,V$ of density 2.60 $mA\,cm^{-2}$ and a shoulder peak around $-1.33\,V$ of density 3.65 $mA\,cm^{-2}$. The j–E curve recorded on a GC substrate electrode under the same conditions is also displayed in Fig. 5. The current is negligible in
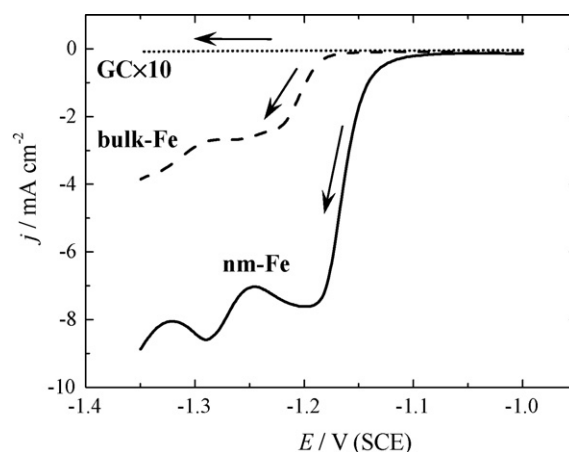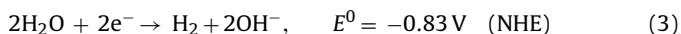

Fig. 7. Comparison of catalytic activity between nm-Fe/GC electrode (—), bulk-Fe electrode (- - -) and GC electrode (......), j–E curves recorded in $0.01\,mol\,L^{-1}$ NaNO2 + $0.2\,mol\,L^{-1}$ NaOH solution, scan rates $1\,mV\,s^{-1}$.

comparison with those obtained on both nm-Fe/GC and bulk-Fe electrodes, confirming again that the GC surface is inert for nitrite reduction and does affect the determination of catalytic activity of Fe cuboid nanoparticles supported on it. These results illustrate clearly that the electrocatalytic activity of Fe nanocubes is much higher than that of the bulk Fe.

It is interesting to mention that during nitrite reduction with a scan rate of $1\,mV\,s^{-1}$ the evolution of gas bubbles can be observed by naked eye on both nm-Fe/GC and bulk-Fe electrodes. The most possible gas products generated in electroreduction of nitrite under present conditions may be gaseous NO and H_2 according to [45], i.e.

$$NO_2^- + H_2O + e^- \rightarrow NO + 2OH^-, \qquad E^0 = 0.46\,V \quad (NHE) \qquad (2)$$
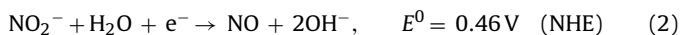
together with hydrogen evolution,

$$2H_2O + 2e^- \rightarrow H_2 + 2OH^-, \qquad E^0 = -0.83\,V \quad (NHE) \qquad (3)$$

It is nevertheless possible that other species may be produced in electroreduction of nitrite, such as N_2, H_2N–OH, H_2N–NH_2, and NH_3. The exact products will depend on the reduction conditions, such as pH, electrolyte, reduction potential, electrode materials, etc. In situ FTIR spectroscopy may reveal the chemical nature of products at molecule level, which is conducted under investigation.

In order to study the steady catalytic activity, j–t curves of nitrite reduction on nm-Fe/GC and bulk-Fe electrodes were recorded by applying the following procedure: (1) electrode potential was held at $-0.8\,V$ for $3.0\,s$ to establish a equilibrium state of electrochemical system; (2) the electrode potential was then stepped negatively to -1.2, -1.25, and $-1.3\,V$, respectively, and stayed at each potential for $300.0\,s$ to reduce nitrite. Meanwhile the j–t (0–$300\,s$) curves were recorded. Fig. 8 displays the j–t curves recorded on nm-Fe/GC and bulk-Fe electrodes. It can be observed that on both electrodes the steady current of nitrite reduction is achieved after $50\,s$. The steady current measured on nm-Fe/GC is always 2.4–3.3 times larger than that acquired on bulk-Fe at the same reduction potential, i.e. at $-1.20\,V$, $j_{nm-Fe/GC}/j_{bulk-Fe} = 5/1.5 = 3.3$; at $-1.25\,V$, $j_{nm-Fe/GC}/j_{bulk-Fe} = 7/2.5 = 2.8$; and at $-1.30\,V$, $j_{nm-Fe/GC}/j_{bulk-Fe} = 8/3.4 = 2.4$. A visible fluctuation of j is observed in j–t curves recorded on nm-Fe/GC, such fluctuation is not obvious in j–t curves obtained on bulk Fe, which may be due to the influence of gas evolution during nitrite reduction. Since, as seen above, the reduction on nm-Fe/GC is faster than that on bulk Fe, which leads the influence more pronounced on the nm-Fe/GC electrode.

The present results demonstrated clearly that Fe cuboid nanoparticles exhibited a much higher catalytic activity per unit
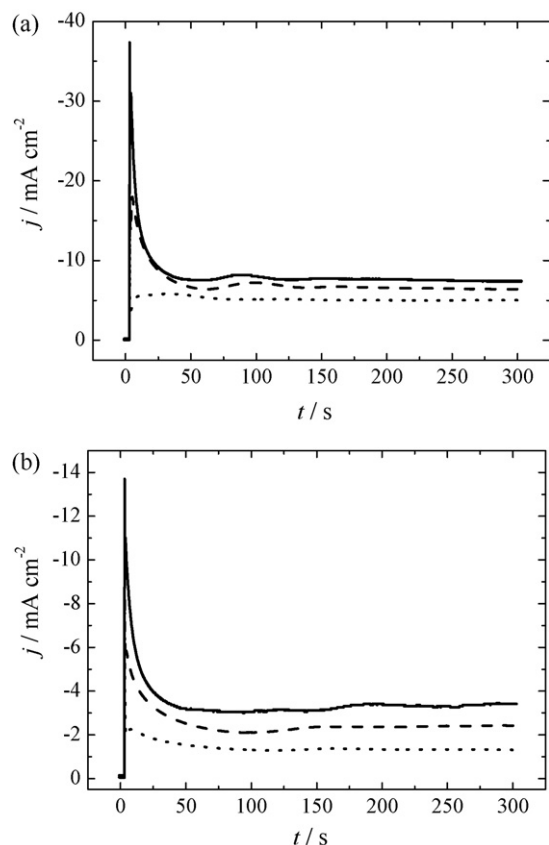
Fig. 8. *j–t* Curves recorded on nm-Fe/GC (a) and bulk Fe (b) electrodes, 0.01 mol L^{-1} NaNO$_2$ + 0.2 mol L^{-1} NaOH solution, reduction potentials, respectively, at −1.20 V (. . . . . .), −1.25 V (- - -), and −1.30 V (—).

surface area than that of bulk Fe towards electroreduction of nitrite. This enhanced catalytic activity may be originated from the open structure of the bcc {1 0 0} facets of the Fe nanocubes, and may be also attributed to the size effects of Fe cuboid nanoparticles.

4. Conclusions

The current paper has put emphasis upon shape control synthesis of Fe nanoparticles and their electrocatalytic properties. Fe cuboid nanoparticles supported on glassy carbon were prepared by electrochemical deposition under cyclic voltammetric conditions. The results of SEM, XRD, SAED and EDX analysis confirmed that the Fe nanoparticles are Fe single crystals of cube shape and distributed discretely on GC substrate with an average size of 171 nm. It has revealed by cyclic voltammetric studies that the Fe cuboid nanoparticles exhibited a much higher catalytic activity towards nitrite reduction. In comparison with the data measured on a-Fe bulk electrode, the onset potential of nitrite reduction on nm-Fe/GC electrode has been shifted positively about 100 mV, and the steady reduction current density is 2.4–3.3 times larger. The better catalytic properties of the nm-Fe/GC electrode have been attributed to the open structure of bcc {1 0 0} facets of Fe nanocubes and also to the nanosize effect of Fe nanoparticles.

References

[1] V.M. Shalaev, A.K. Sarychev, Phys. Rev. B 57 (1998) 13265.
[2] V. Palermo, M. Palma, P. Samori, Adv. Mater. 18 (2006) 145.
[3] L. Krusin-Elbaum, T. Shibauchi, B. Argyle, L. Gignac, D. Weller, Nature 410 (2001) 444.
[4] V.N. Balbyshev, D.J. King, A. Khramov, L.S. Kasten, M.S. Donley, Thin Solid Films 447 (2004) 558.
[5] K.W. Park, J.H. Choi, Y.E. Sung, J. Phys. Chem. B 107 (2003) 5851.
[6] P.V. Kamat, S. Barazzouk, S. Hotchandani, K.G. Thomas, Chem. Eur. J. 6 (2000) 3914.
[7] S.G. Sun, in: A. Wieckowski, E. Savinova, C.G. Vayenas (Eds.), Catalysis and Electrocatalysis at Nanoparticle Surfaces, Marcel Dekker, Inc., New York, 2003, p. 785 (Chapter 21).
[8] N.D. Spencer, R.C. Schoonmaker, G.A. Somorjai, Nature 294 (1981) 643.
[9] S. Dahl, A. Logadottir, C.J.H. Jacobsen, J.K. Norskov, Appl. Catal. A-Gen. 222 (2001) 19.
[10] G.A. Somorjai, J.Y. Park, Catal. Lett. 115 (2007) 87.
[11] M. Ouzounidou, A. Skodra, C. Kokkofitis, Solid. State Ionics 178 (2007) 153.
[12] B.A. Till, L.J. Weathers, P.J.J. Alvarez, Environ. Sci. Technol. 32 (1998) 634.
[13] Y.H. Huang, T.C. Zhang, P.J. Shea, S.D. Comfort, J. Environ. Qual. 32 (2003) 1306.
[14] J.L. Ginner, P.J.J. Alvarez, S.L. Smith, M.M. Scherer, Environ. Eng. Sci. 21 (2004) 219.
[15] K.C. Huang, K.S. Chou, Electrochem. Commun. 9 (2007) 1907.
[16] F. He, D.Y. Zhao, Environ. Sci. Technol. 41 (2007) 6216.
[17] R.J. Joseyphus, D. Kodama, T. Matsumoto, Y. Sato, B. Jeyadevan, K. Tohji, J. Magn. Magn. 310 (2007) 2393.
[18] Z.L. Wang, J. Phys. Chem. B 104 (2000) 1153.
[19] H.J. Song, F. Kim, S. Connor, G.A. Somorjai, P.D. Yang, J. Phys. Chem. B 109 (2005) 188.
[20] N. Tian, Z.Y. Zhou, S.G. Sun, Y. Ding, Z.L. Wang, Science 316 (2007) 732.
[21] O. Margeat, F. Dumestre, C. Amiens, B. Chaudret, P. Lecante, M. Respaud, Prog. Solid State Chem. 33 (2005) 71.
[22] D. Kim, J. Park, K. An, N.K. Yang, J.G. Park, T. Hyeon, J. Am. Chem. Soc. 129 (2007) 5812.
[23] X. Liang, X. Wang, J. Zhuang, Y.T. Chen, D.S. Wang, Y.D. Li, Adv. Funct. Mater. 16 (2006) 1805.
[24] T.J. Park, S.S. Wong, Chem. Mater. 18 (2006) 5289.
[25] K. Rajeshwar, J.G. Ibanez, Environmental Electrochemistry—Fundamentals and Applications in Pollution Abatement, Academic Press, San Diego, 1997.
[26] T. Hiratsu, S. Suzuki, K. Yamaguchi, Chem. Commun. 36 (2005) 4534.
[27] C. Polatides, M. Dortsiou, G. Kyriacou, Electrochim. Acta 50 (2005) 5237.
[28] O. Brylev, M. Sarrazin, L. Roué, D. Bélanger, Electrochim. Acta 52 (2007) 6237.
[29] K. Tada, K. Shimazu, J. Electroanal. Chem. 577 (2005) 303.
[30] K. Tada, T. Kawaguchi, K. Shimazu, J. Electroanal. Chem. 572 (2004) 93.
[31] I.G. Casella, M. Gatta, J. Electroanal. Chem. 568 (2004) 183.
[32] S.E. Bae, K.L. Stewart, A.A. Gewirth, J. Am. Chem. Soc. 129 (2007) 10171.
[33] S.N. Pronkin, P.A. Simonov, V.I. Zaikovskii, E.R. Savinova, J. Mol. Catal A: Chem. 265 (2007) 141.
[34] Y. Tian, J.X. Wang, Z. Wang, S.C. Wang, Synth. Met. 143 (2004) 309.
[35] S.M. Chen, S.H. Hsueh, J. Electrochem. Soc. 150 (2003) D175.
[36] J.E. Toth, F.C. Anson, J. Am. Chem. Soc. 111 (1989) 2444.
[37] Q.S. Chen, S.G. Sun, et al., Langmuir 22 (2006) 10575.
[38] Z.L. Xiao, C.Y. Han, W.K. Kwok, H.H. Wang, U. Welp, J. Wang, G.W. Crabtree, J. Am. Chem. Soc. 126 (2004) 2316.
[39] A. Cuesta, C. Gutiérrez, J. Phys. Chem. 100 (1996) 12600.
[40] J. O'M. Bockris, S.U.M. Khan, Surface Electrochemistry: A Molecular Level Approach, Plenum Press, New York and London, 1993.
[41] L.D. Burke, O.J. Murphy, J. Electroanal. Chem. 109 (1980) 379.
[42] G. Larramona, C. Gutiěrrez, J. Electrochem. Soc. 136 (1989) 2171.
[43] C. Gutiérrez, B. Beden, J. Electroanal. Chem. 293 (1990) 253.
[44] S.G. Sun, A.C. Chen, Electrochim. Acta 39 (1994) 969.
[45] A.J. Bard, R. Parsons, J. Jordan (Eds.), Standard Potentials in Aqueous Solutions, Marcel Dekker, New York, 1985.